Publ. Astron. Soc. Japan (2020) 72 (4), 63 (1–15)
doi: 10.1093/pasj/psaa040
Advance Access Publication Date: 2020 June 11

86-GHz SiO masers in Galactic centre OH/IR stars

Maria Messineo,[1,3,*] Lorant O. Sjouwerman,[2] Harm J. Habing,[3] and Alain Omont[4]

[1]Key Laboratory for Researches in Galaxies and Cosmology, University of Science and Technology of China, Chinese Academy of Sciences, Hefei, Anhui, 230026, China
[2]National Radio Astronomy Observatory, PO Box O, Socorro, NM 87801, USA
[3]Leiden Observatory, PO Box 9513, 2300 RA Leiden, the Netherlands
[4]Institut d'Astrophysique de Paris, CNRS, 98bis boulevard Arago, 75014 Paris, France

*E-mail: maria.messineo@hotmail.com

Received 2019 October 24; Accepted 2020 April 12

Abstract

We present results on a search for 86.243-GHz SiO ($J = 2\rightarrow1$, $v = 1$) maser emission toward 67 OH/IR stars located near the Galactic centre. We detected 32 spectral peaks, of which 28 correspond to SiO maser lines arising from the envelopes of these OH/IR stars. In OH/IR stars, we obtained an SiO maser detection rate of about 40%. We serendipitously detected two other lines from OH/IR stars at ≈86.18 GHz, which could be due to a CCS-molecule transition at 86.181 GHz or probably to an highly excited OH molecular transition at 86.178 GHz. The detection rate of 86-GHz maser emission is found to be about 60% for sources with the Midcourse Space Experiment (MSX) $A - E < 2.5$ mag; but it drops to 25% for the reddest OH/IR stars with MSX $A - E > 2.5$ mag. This supports the hypothesis by Messineo (2002, A&A, 393, 115) that the SiO masers are primarily found in relatively thinner circumstellar material.

Key words: circumstellar matter — Galaxy: stellar content — infrared: stars — masers — stars: late-type

1 Introduction

At the end of their life, asymptotic giant branch (AGB) stars ($\approx 1 < M_* < \approx 8\,M_\odot$) enter a phase of intense mass loss at rates of typically 10^{-7} to $10^{-4}\,M_\odot\,\mathrm{yr}^{-1}$ (Herwig 2005). A variety of names are used in literature to indicate thermal pulsing AGB stars, either referring to their pulsation properties (e.g., semiregular, Miras, long-period variables), or to their envelope properties (optically thick or thin envelopes), or masers. Indeed, their circumstellar envelopes can exhibit maser emission (e.g., from SiO, H_2O, and OH molecules; Habing 1996). SiO maser emission originates close to the stellar photosphere, inside the dust formation zone. H_2O maser spots form further out, in the acceleration region, and 1612-MHz OH masers originate in the cooler part of the envelope where the expanding shell has reached a terminal velocity (known as V_{exp}). van der Veen and Habing (1988) and Lewis (1989) analyzed the colors of IRAS sources, and suggested an evolutionary sequence of increasing mass-loss rate and maser occurrence (from SiO, via H_2O, to OH masers) with redder colors. More recently, instead of a sequence of mass-loss rate, Sjouwerman et al. (2009) interprets this sequence to be more likely a shell thickness or shell density estimator. Regardless, the observed sequence indicates an empirical stellar type; it goes from shell-less evolved late-type stars, Mira-type stars with thin shells and silicate features in emission, through optically obscured thick-shell OH/IR stars with silicate features in absorption, and ends in planetary nebulae. SiO maser transitions are easily detected at 43 GHz ($J = 1 \rightarrow 0$, $v = 1$ and $v = 2$) and at 86 GHz ($J = 2 \rightarrow 1$, $v = 1$) toward oxygen-rich AGBs, typically in objects with the silicate feature in emission. The relative strength of the SiO maser lines varies with source type (Mira versus OH/IR; Lane 1982; Nyman et al. 1986, 1993), suggesting that the SiO maser pumping mechanism strongly depends on mass-loss rate (shell thickness) and luminosity; individually, line ratios also vary with stellar pulsation phase (Stroh et al. 2018). Note that the classic term "Mira" indicates optically visible long-period variables ($> \approx 100$ d) with large amplitudes, while, today, the term "OH/IR star" is often used to indicate optically thick long-period variables (LPVs) with mass-loss rates above $10^{-5}\,M_{\odot}\,\mathrm{yr}^{-1}$, independently of masers (e.g., Blommaert et al. 2018; Habing 1996) even though they were discovered and classified because of OH maser emission.

Here, we present spectra of 86-GHz SiO maser lines of a sample of 67 OH/IR stars with OH maser emission. The data set was obtained using the IRAM 30-m telescope and the data analysis was carried out in the year 2002. Since the strength and occurrence of masers vary in phase with the infrared stellar pulsation cycle of these long-period variables, it is valuable to perform and keep track of repeated observations. The main purpose of this communication is to provide an historical record for these detections, as the raw data are not stored in any archive. This dataset was taken to verify the hypothesis made by Messineo et al. (2002) on their color selection of targets for the 86-GHz SiO maser search. The authors selected Mira-like stars with bluer color to avoid genuine OH/IR stars, and any known OH emitter was removed from their list. This avoidance was based on the idea that SiO maser emission was more likely to occur (and perhaps more strongly) in relatively thin-shell Miras than in thick-shell OH/IR stars. Evidence was based, though, on few observations (Messineo et al. 2002 and references therein).

Along with the SiO masers towards OH/IR stars, a few other serendipitously detected lines are reported. In section 2 we describe the sample and observations. In section 3, the 86-GHz detections are presented and commented on where appropriate.

2 The sample and 86-GHz observations

The list of 67 AGB OH/IR stars observed is presented in tables 1 (detections) and 2 (non-detections). This sample of sources comes from the catalogues of OH/IR stars near the Galactic centre (GC) from Lindqvist et al. (1992) (comprising 134 sources), with additional sources from Sjouwerman et al. (1998). These OH/IR stars are among the brightest and reddest infrared sources and had already been detected with the IRAS mid-infrared satellite (Habing 1996). The targeted OH/IR stars were selected on the basis of having ISOGAL measurements at 7 and 15 μm (Ortiz et al. 2002), i.e., they are located in fields observed with ISOCAM on board the ESA/ISO satellite (Omont et al. 2003; Schuller et al. 2003).

At the time of these observations, the sample of OH/IR stars by Lindqvist comprised 134 stars concentrated in the central one degree. The sample of bulge + disk OH/IR stars from the blind survey of Sevenster et al. (1997, 2001) comprised only about 700 sources[1]. Furthermore, the Lindqvist sample had been re-identified with ISOGAL data. Therefore, due to the stellar density distribution and available data, it was straightforward to compare our comprehensive Mira-like sample towards the inner Galaxy, with a sample of OH/IR stars on the Galactic centre.

The observations were carried out with the IRAM 30-m telescope (Pico Veleta, Spain) between 2001 December and 2002 April (15 hr awarded to IRAM program 144-01, P.I. Messineo). The observing technique and setup as well as the data reduction and analysis were identical to those described by Messineo et al. (2002). The IRAM pointing coordinates were based on the Deep Near Infrared Survey of the southern sky (DENIS) and typically accurate within 1″ (Epchtein et al. 1994). IRAM telescope pointing errors are typically within 2″–4″, while the 86-GHz beam full-width at half-maximum (FWHM) is 29″. Two orthogonal linear polarized receivers were tuned to simultaneously observe the SiO maser line at a rest frequency of 86.24335 GHz ($J = 2 \rightarrow 1$, $v = 1$). The receiver output was combined to obtain total intensity spectra. For each receiver, we used in parallel the low-resolution filter bank (3.5 km s^{-1} spectral resolution and 890 km s^{-1} total velocity coverage) and the autocorrelator (1.1 km s^{-1} of resolution and 973 km s^{-1} of coverage). Observations were made in wobbler switching mode with a wobbler throw of 100″–200″. The individual on-source integration time was set between 12 and 24 minutes per source, depending on the system temperature (110–250 K). The conversion factor from antenna temperature to flux density is 6.2 Jy K^{-1}.

3 Detected lines

In order to measure the emission from the maser lines, a linear baseline was subtracted from the spectra. This was a detection project and the typical signal-to-noise ratio threshold of detection for the expected velocity resolution

[1] More recently, Engels and Bunzel (2015) reported on 2341 stars with OH masers. There is an ongoing new survey of the Galactic plane, and Qiao et al. (2018) reported on 161 new OH masers in the central 5°.

Table 1. Compilation of parameters and aliases of OH/IR stars detected at 86 GHz.

ID†	RA‡ [J2000.0]	Dec‡ [J2000.0]	V_{LSR} [km s^{-1}]	T_a [K]	rms [K]	A [K km s^{-1}]	FWHM [km s^{-1}]	Obs. date [yymmdd]	Alias1+	— Engels and Bunzel (2015) — Alias2	V_{LSR}‖ [km s^{-1}]	V_{exp}‖ [km s^{-1}]	Per [d]	Δ K [mag]	References♯	Note
1	17:44:28.391	−29:26:33.76	*(414.31)*	0.104	0.014	0.54 ± 0.08	11.15 ± 2.41	011214/ 020326	LI004	OH359.437−0.051	−138.20	15.30	..	..	1,3,4	"SiO"(?) velocity differs from OH
2	17:44:34.987	−29:04:35.47	−6.08	0.133	0.015	0.51 ± 0.03	3.46 ± 0.27	020326	LI033	OH359.762+00.12	−5.55	14.73	..	..	1,5	
3	17:44:39.721	−29:16:45.88	−73.43	0.085	0.021	0.23 ± 0.06	2.43 ± 0.73	011219	LI014	OH359.598+0.000	−73.75	19.05	664	2.30	1,3,4,5	
4	17:44:46.003	−29:06:13.61	−58.23	0.047	0.013	0.17 ± 0.05	3.75 ± 1.20	020319	LI032	OH359.760+0.072	−54.90	20.60	676	2.09	1,3,4	
5	17:44:51.262	−29:09:45.58	−103.85	0.089	0.022	0.51 ± 0.12	6.77 ± 1.99	020319	LI027	OH359.719+0.025	−102.35	22.25	669	1.79	1,3,4	
6	17:44:56.881	−29:13:25.36	−148.39	0.053	0.033	0.49 ± 0.06	7.17 ± 1.00	020326	LI022	OH359.68−0.02	−149.97	21.63	..	..	1,5	
7	17:45:03.241	−29:07:12.69	−26.72	0.078	0.019	0.35 ± 0.07	5.33 ± 1.08	020319	LI038	OH359.778+0.010	−27.95	21.05	572	1.19	1,3,4,6,7	
8	17:45:05.333	−29:17:13.31	−140.78	0.077	0.013	0.45 ± 0.10	5.69 ± 1.71	011221	LI018	OH359.640−0.084	−141.65	14.45	546	0.91	1,3,4	
9	17:45:11.549	−28:38:37.36	*(154.69)*	0.064	0.013	0.32 ± 0.09	3.60 ± 1.15	020319	LI101	OH0.200+0.233	−67.05	15.85	825	2.43	1,3,4,5	86.178-GHz OH $V_{LSR}\sim -65$ km s^{-1}
10	17:45:12.959	−29:12:54.58	28.68	0.098	0.011	0.32 ± 0.12	3.54 ± 2.35	011229	LI026	OH359.716−0.070	29.40	22.25	691	1.94	1,3,4	
11	17:45:13.942	−28:47:43.22	21.07	0.055	0.009	0.20 ± 0.03	3.36 ± 0.58	020328	LI086	OH008+0.15	21.83	21.03	616	2.24	1,7	
12	17:45:13.988	−29:06:56.30	−12.60	0.069	0.015	0.23 ± 0.05	2.98 ± 0.79	020319	LI042	OH359.803−0.021	−13.45	22.40	838	0.90	1,3,4	
13	17:45:14.303	−29:07:20.78	−72.35	0.027	0.005	0.28 ± 0.05	7.00 ± 1.28	020328	Sj004	OH359.797−0.025	−71.20	19.30	547	2.01	2,5,6,7	
14	17:45:17.870	−29:05:53.63	−53.88	0.065	0.023	0.24 ± 0.04	3.70 ± 0.53	020326	LI047	OH359.83−0.02	−52.97	20.63	660	1.56	1,5,6,7	
15	17:45:19.358	−29:14:05.94	−28.89	0.058	0.011	0.21 ± 0.08	3.35 ± 1.45	011229	LI025	OH359.711−0.100	−32.10	19.45	686	1.38	1,3,4,5	
16	17:45:29.397	−28:39:35.03	62.35	0.036	0.013	0.16 ± 0.04	4.07 ± 1.25	020319	LI104	OH0.221+0.168	61.80	19.20	697	2.48	1,3,4,5	
17	17:45:31.502	−28:46:22.04	−53.88	0.053	0.011	0.15 ± 0.03	2.66 ± 0.67	020326	LI091	OH0.13+0.10	−52.37	11.40	458	..	1	
18	*17:45:32.089*	*−28:46:19.42*	43.89	0.047	0.011	0.24 ± 0.05	5.75 ± 1.73	020326	V*V4502Sgr	..	..	..	..	..		In beam of LI091 (#17)
19	17:45:34.833	−29:06:02.45	3.69	0.076	0.020	0.49 ± 0.08	5.21 ± 1.05	020319	LI050	OH359.855−0.078	4.10	21.85	611	1.64	1,3,4,6	
20	17:45:34.833	−29:06:02.45	*(222.04)*	0.062	0.020	0.45 ± 0.10	7.77 ± 2.13	020319			..	..	..	..	..	86.178-GHz OH $V_{LSR}\sim +2$ km s^{-1}
21	17:45:48.497	−29:10:45.01	−31.07	0.068	0.017	0.20 ± 0.05	2.69 ± 0.94	020319	LI045	OH359.814−0.162	−31.70	20.40	547	1.85	1,3,4,6,7	
22	17:45:56.130	−28:39:27.00	102.55	0.056	0.013	0.21 ± 0.04	3.56 ± 0.75	020319	LI109	OH0.274+0.086	103.00	24.40	706	2.13	1,3,4	
23	17:46:15.001	−28:44:17.31	37.37	0.043	0.013	0.16 ± 0.19	3.64 ± 5.39	020319	LI106	OH0.241−0.014	35.00	18.35	535	0.94	1,3,4	
24	17:46:19.597	−29:00:41.72	8.04	0.043	0.013	0.19 ± 0.04	4.01 ± 0.69	020331	Sj073	OH0.016−0.171	8.20	19.30	581	2.70	2,7	
25	17:46:22.161	−28:46:22.51	−109.28	0.044	0.014	0.15 ± 0.05	4.78 ± 1.27	020319	LI105	OH0.225−0.055	−106.15	16.60	525	1.52	1,3,4,7	
26	17:46:28.757	−28:53:19.54	41.71	0.054	0.014	0.27 ± 0.12	4.69 ± 2.42	020319/ 020328	LI094	OH0.138−0.136	40.20	21.10	810	1.40	1,3,4,5	

Table 1. (Continued)

ID†	RA‡ [J2000.0]	Dec‡ [J2000.0]	V_{LSR} [km s^{-1}]	T_a [K]	rms [K]	A [K km s^{-1}]	FWHM [km s^{-1}]	Obs. date [yymmdd]	Alias1+	— Engels and Bunzel (2015) — Alias2	V_{LSR}‖ [km s^{-1}]	V_{exp}‖ [km s^{-1}]	Per [d]	Δ K [mag]	References♯	Note
27	17:46:31.282	−28:39:48.49	38.45	0.095	0.015	0.39 ± 0.07	3.89 ± 0.81	020319	LI113	OH0.336−0.027	38.00	17.00	514	1.01	1,3,4	
28	17:46:33.150	−28:45:00.61	13.47	0.110	0.020	0.53 ± 0.08	4.54 ± 0.71	020319	LI108	OH0.265−0.078	12.15	17.75	595	1.13	1,3,4	
29	17:46:38.540	−29:08:03.48	146.00	0.049	0.010	0.09 ± 0.02	1.74 ± 0.55	020331	Sj041	OH359.947−0.294	143.90	21.10	..	..	2	
30	17:47:02.211	−28:45:55.84	−10.43	0.084	0.016	0.35 ± 0.06	4.32 ± 0.89	020319	LI110	OH0.307−0.176	−8.50	20.40	657	1.56	1,3,4	
31	17:47:21.298	−28:39:23.26	92.77	0.038	0.014	0.23 ± 0.05	5.54 ± 1.23	020319	LI119	OH0.437−0.179	96.20	17.60	744	2.31	1,3,4	
32	17:47:24.052	−28:32:43.01	147.08	0.060	0.010	0.32 ± 0.04	4.76 ± 0.68	011219/ 020206	LI127	OH0.536−0.130	146.20	23.30	669	1.48	1,3,4	

†Supplementary information: (a) At the location of OH359.437−0.051 (LI004, ID = 1) we detected a broad high-velocity line at $V_{LSR} = 414.31\,\mathrm{km\,s^{-1}}$ (FWHM = $11.16\,\mathrm{km\,s^{-1}}$), assuming a rest frequency of the SiO transition. The actual 1612 MHz OH maser velocity is $V_{LSR} = -138.20\,\mathrm{km\,s^{-1}}$, and its corresponding anticipated SiO maser is not detected at 86 GHz around this 1612-MHz OH velocity. LI004 is the brightest mid-infrared star with [4.5] = 10.4 mag, [8.0] = 6.1 mag, [15.0] = 4.24 mag. Only two other 8-μm GLIMPSE stars fall within the IRAM telescope beam, but they are much fainter with [8.0] = 7.70 and 7.80 mag. With a rest frequency of about 86.084 GHz (which is uncertain to a few MHz), the nature of this serendipitous line is undetermined. (b) At the position of the OH/IR star LI101/OH0.200+0.233 we detected a line at V_{LSR}=154.69 km s^{-1} (FWHM = 3.6 km s^{-1}), while the 1612 MHz OH maser line is at $V_{LSR} = -67.40\,\mathrm{km\,s^{-1}}$. We think that this is a detection of OH instead of SiO; see the note further down. (c) The velocities of two detected lines (ID = 9 and 20) differ from the expected LI101 and LI050 1612-MHz OH maser velocities by about 220 km s^{-1} when assuming they originate as the SiO ($v = 1$, $J = 2 \rightarrow 1$) maser. Alternatively it suggests a possible line from the targeted source at a frequency of about 86.18 GHz. We propose these detections, instead of from SiO, originate from an highly excited OH $^2\Pi_{3/2}$ $J = \frac{17}{2}$ ($v = 1$) $F = 8^+$–8^- main line transition at 86.178 GHz. There are no other bright mid-infrared stars ([8.0] < 8.9 mag) at these positions. (d) We serendipitously detected another SiO maser when pointing to OH0.129+0.103 (ID = #17, LI091). The OH/IR star has $V_{LSR} = -52.75\,\mathrm{km\,s^{-1}}$ and coincides with ISOGAL-P J174534.8−290602, the brightest 15-μm star (3.6 mag; Ortiz et al. 2002). The second maser (V_{LSR}=43.89 km s^{-1}, ID = #18) detected in the same beam likely belongs to the known long-period variable V* V4502 Sgr (8.″8 distant). Both variables are detected by GLIMPSE with [8.0] = 5.47 and 6.65 mag, and [3.6 − 8.0] = 1.66 and 0.63 mag, respectively. (e) 3.69 km s^{-1} (FWHM = 5.21 km s^{-1}) and another line at $V_{LSR} = 222.04\,\mathrm{km\,s^{-1}}$ (FWHM = 7.77 km s^{-1}). The 3.69 km s^{-1} line is an SiO detection of OH359.855−0.078 with a 1612-MHz OH maser velocity detemined at $V_{LSR} = 3.95\,\mathrm{km\,s^{-1}}$ (Lindqvist et al. 1992). In addition to SiO we think we also detect OH in this object; see the next note below.

‡IRAM telescope pointing coordinates.

§Alias names are taken from Ortiz et al. (2002) and SIMBAD.

‖V_{LSR} and V_{exp} are from the 1612-MHz OH measurements and are the average of the measurements listed in the catalog of Engels and Bunzel (2015).

♯References: 1—Lindqvist et al. (1992), 2—Sjouwerman et al. (1998), 3—Wood, Habing, and McGregor (1998), 4—Ortiz et al. (2002), 5—Vanhollebeke et al. (2006), 6—Glass et al. (2001), 7—Matsunaga et al. (2009).

Table 2. Compilation of parameters and aliases of OH/IR stars undetected at 86 GHz.

ID	RA* [J2000.0]	Dec* [J2000.0]	rms [K]	Obs. date [yymmdd]	Alias1[†]	— Engels and Bunzel (2015) — Alias2	V_{LSR}[‡] [km s^{-1}]	V_{exp}[‡] [km s^{-1}]	Per [d]	Δ K [mag]	References[§]
33	17:43:45.521	−29:26:16.22	0.012	020326	LI001	OH359.360+00.08	−211.50	12.33	..	..	1
34	17:43:54.019	−29:25:23.41	0.012	020326	LI002	OH359.388+0.066	−129.10	17.60	..	..	1
35	17:44:14.988	−28:45:05.98	0.018	020326	LI076	OH000.000+00.35	124.03	9.40	477	1.06	1,3,5
36	17:44:34.541	−29:10:37.17	0.018	011221	LI021	OH359.68+0.07	−24.50	18.67	698	2.05	1,3,4,5
37	17:44:44.462	−29:05:38.29	0.013	020319	LI035	OH359.765+0.082	110.95	17.60	552	2.22	1,3,4,5
38	17:44:47.983	−29:06:49.82	0.014	020319	LI031	OH359.755+0.061	37.90	18.75	..	..	1,3,4,5
39	17:44:54.199	−29:13:44.94	0.018	011221	LI020	OH359.669−0.019	−83.80	17.50	481	1.01	1,3,4,5
40	17:44:57.779	−29:20:42.50	0.015	011219	LI012	OH359.576−0.091	−55.50	18.60	672	2.94	1,3,4,5
41	17:45:01.740	−29:02:49.99	0.022	020401	Sj011	OH359.838+0.052	−68.20	12.30	444	0.85	2,5,6
42	17:45:06.992	−29:03:34.16	0.014	020319	LI048	OH359.837+0.030	−75.35	7.95	399	1.07	1,3,4,5,6,7
43	17:45:10.467	−29:18:11.77	0.017	011219	LI017	OH359.636−0.108	−138.05	22.30	847	2.73	1,3,4
44	17:45:12.480	−28:40:44.11	0.014	020319	LI096	OH0.173+0.211	46.40	17.05	514	1.57	1,3,4,5
45	17:45:13.109	−29:09:36.19	0.014	011214	LI034	OH359.763−0.042	120.30	13.90	457	1.24	1,3,4,6
46	17:45:13.890	−29:15:28.55	0.017	020319	LI023	OH359.681−0.095	−98.85	19.45	759	2.95	1,3,4
47	17:45:16.460	−29:15:37.55	0.010	020206	LI024	OH359.684−0.104	−59.35	16.85	535	1.26	1,3,4
48	17:45:18.119	−29:18:04.03	0.017	011221	LI019	OH359.652−0.131	−188.35	20.35	671	2.03	1,3,4
49	17:45:29.279	−29:07:04.22	0.008	020331	Sj008	OH359.830−0.070	−82.70	18.20	567	1.36	2,6,7
50	17:45:29.508	−29:09:16.60	0.015	020328	LI040	OH359.80−0.09	−3.90	17.97	626	2.40	1,5,7
51	17:45:33.331	−29:11:23.17	0.029	020326	LI037	OH359.78−0.12	71.80	13.03	284	1.00	1,6
52	17:45:33.449	−28:43:45.08	0.012	020331	Sj001	OH0.170+0.119	116.00	22.70	999	1.86	2,7
53	17:45:34.439	−29:12:54.22	0.026	020401	Sj002	OH359.757−0.136	−10.80	20.30	..	..	2,5
54	17:45:46.609	−28:32:40.13	0.014	020319	LI115	OH0.352+0.175	10.80	18.20	661	2.24	1,3,4
55	17:45:54.228	−28:31:46.74	0.014	020319	LI116	OH0.379+0.159	139.30	15.30	985	3.03	1,3,4
56	17:46:01.113	−29:01:24.20	0.019	011214	LI070	OH359.97−0.12	−8.37	19.30	..	..	1,3,4
57	17:46:11.722	−28:59:32.10	0.014	020401	Sj075	OH0.017−0.137	108.30	18.90	396	1.19	2,6,7
58	17:46:14.529	−28:36:39.49	0.014	020319	LI114	OH0.349+0.053	31.80	14.20	669	2.26	1,3,4
59	17:46:15.407	−28:55:42.71	0.075	020326	LI087	OH0.08−0.12	50.83	14.20	..	..	1
60	17:46:15.840	−28:56:32.39	0.025	020331	SJ092	OH0.067−0.123	35.70	17.40	534	1.30	2,6,7
61	17:46:24.790	−29:00:02.38	0.014	020319	LI080	OH0.036−0.182	152.80	18.50	669	2.60	1,3,4,7
62	17:46:30.737	−28:31:31.87	0.010	011229	LI121	OH0.452+0.046	87.70	10.20	339	0.94	1,3,4
63	17:46:31.780	−28:35:40.81	0.014	020319	LI117	OH0.395+0.008	200.10	13.70	461	1.15	1,3,4
64	17:46:35.478	−28:58:58.98	0.012	020328	LI085	OH000.071−00.20	112.98	13.55	..	..	1
65	17:46:42.330	−28:33:26.14	0.018	020319	LI120	OH0.447−0.006	−186.90	13.10	445	1.85	1,3,4
66	17:46:44.848	−28:34:59.30	0.021	020401	LI118	OH0.430−0.027	31.80	18.70	..	..	1
67	17:46:47.871	−28:47:15.04	0.017	020319	LI107	OH0.261−0.143	25.75	5.55	..	..	1,3,4
68	17:46:59.057	−28:16:58.51	0.027	020328	LI132	OH0.713+0.084	96.80	20.50	..	..	1
69	17:47:39.822	−28:35:48.69	0.013	020326	LI126	OH0.523−0.206	10.80	21.60	1050	2.14	1,3

Notes. *IRAM telescope pointing coordinates.

[†]Alias names are taken from Ortiz et al. (2002) and SIMBAD.

[‡] V_{LSR} and V_{exp} are from the 1612-MHz OH measurements and are the average of the measurements listed in the catalog of Engels and Bunzel (2015).

[§]References: 1—Lindqvist et al. (1992), 2—Sjouwerman et al. (1998), 3—Wood, Habing, and McGregor (1998), 4—Ortiz et al. (2002), 5—Vanhollebeke et al. (2006), 6—Glass et al. (2001), 7—Matsunaga et al. (2009).

is over 2.5–3σ across multiple channels near the centroid of the OH emission in the (1.1 km s^{-1}) autocorrelator spectra. For each line, parameters for e.g., peak and FWHM were estimated using a simple Gaussian fit and are listed in tables 1 and 2.

We searched for 86-GHz SiO maser emission in 67 GC OH/IR stars and detected 32 lines as presented in table 1 and figure 1. A total of 28 OH/IR stars were detected in the SiO ($v = 1$, $J = 2\rightarrow1$) transition at 86.24335 GHz.

SiO maser emission was serendipitously detected from the Mira-type star V4502Sgr (ID = 18 in table 1), which appeared in the beam of ID = #17, LI091. For three positions (ID = 1, 9, 20; alias LI004, LI101, LI050), possible 86-GHz lines are detected at velocities not coincident with

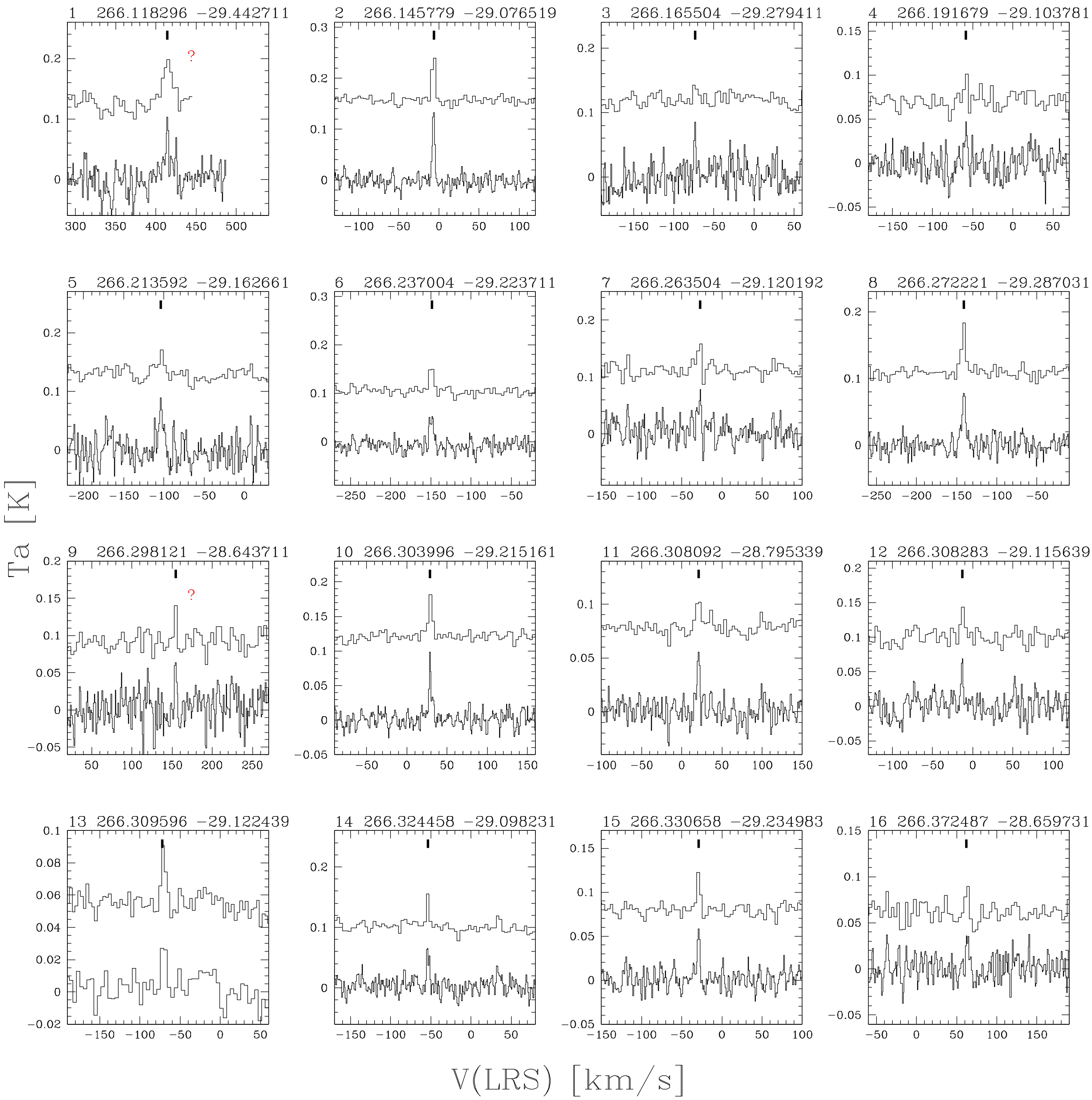

Fig. 1. IRAM spectra of the detected lines. The IDs and observed coordinates (in J2000.0, degrees) are taken from table 1 and printed at the top. In each panel, the spectrum from the auto-correlator (1.1 km s^{-1} channel separation) is plotted at the bottom, while the spectrum from the filterbank (3.5 km s^{-1} channel separation) is plotted at the top. The small black marker at the top shows the derived stellar velocity *using the SiO transition rest frequency*.

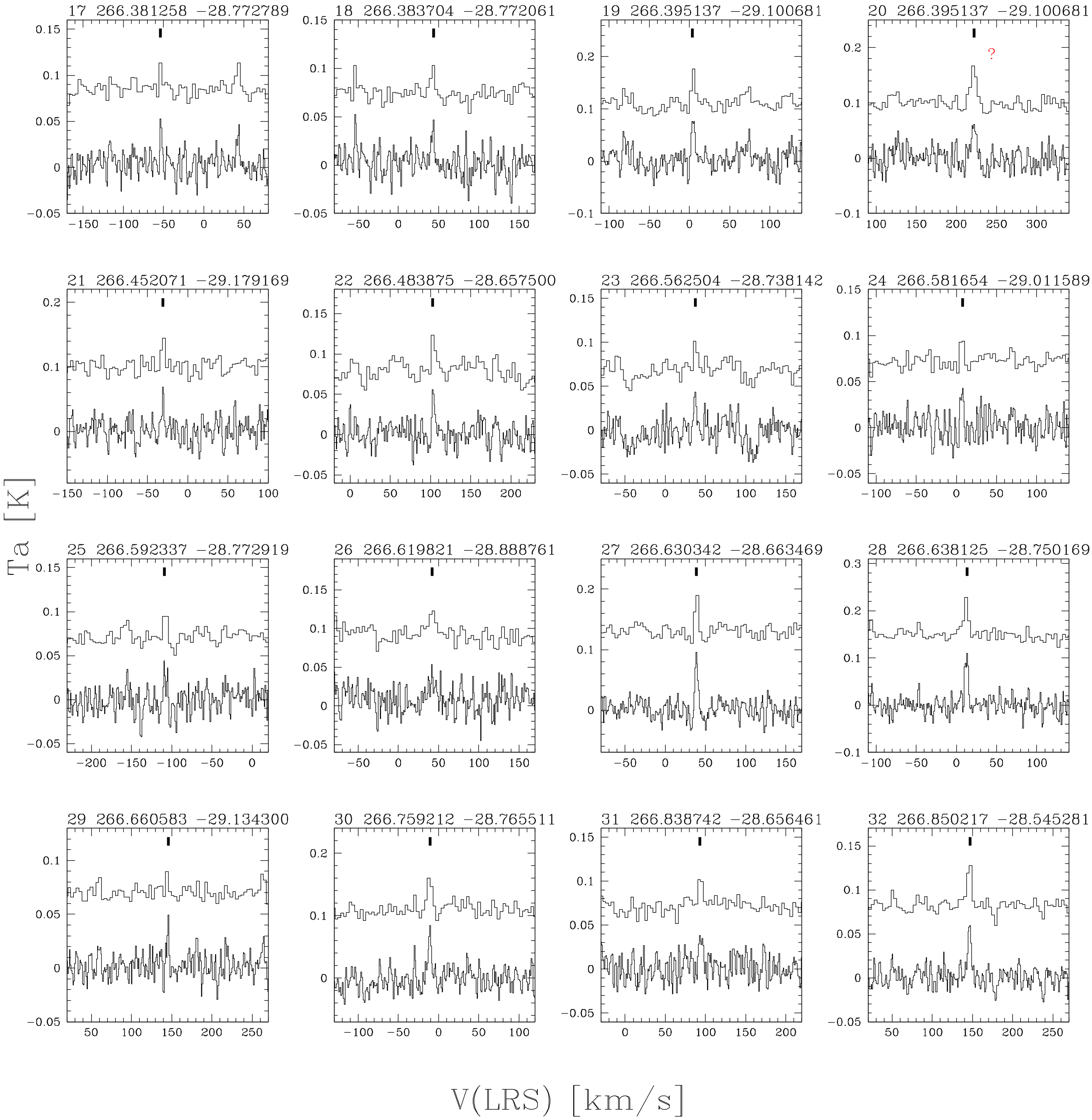

Fig. 1. (Continued)

those expected for the OH/IR stars (figure 2). In these cases, we visually inspected the ISOGAL and GLIMPSE catalogs, but no other bright stars were seen at 8 μm (figure 3). As the offsets from the expected SiO maser velocities of LI101 and LI050 are very similar (i.e., 222 and 218 km s^{-1}) we suggest that these indicate other line detections from the OH/IR stars themselves at a frequency of about 86.18 GHz. A line at 86.181 GHz (a CCS-molecule transition, $J_N = 6_7$–5_6) has been detected towards the carbon AGB star IRC +10216 that is also an OH masing star (Cernicharo et al. 1987; Yamamoto et al. 1990). However, as one of these OH/IR stars has an SiO maser, the association with a carbon-rich star is unlikely (see also Stroh et al. 2018). Because detections of highly excited OH main-line transitions in AGB stars have recently been reported by Khouri et al. (2019), we suggest another highly excited OH transition [e.g., $J = 17/2$ $(v = 1)$ $F = 8^+$–8^- at 86.178 GHz).[2] At the location of LI004 ($V_{\rm LSR} = -138.20$ km s^{-1}), a broad line (FWHM ≈11 km s^{-1}) was detected at $V_{\rm LSR} = +414.3$ km s^{-1} when assuming SiO

[2] See the online catalog of molecular lines at ⟨https://spec.jpl.nasa.gov/⟩.

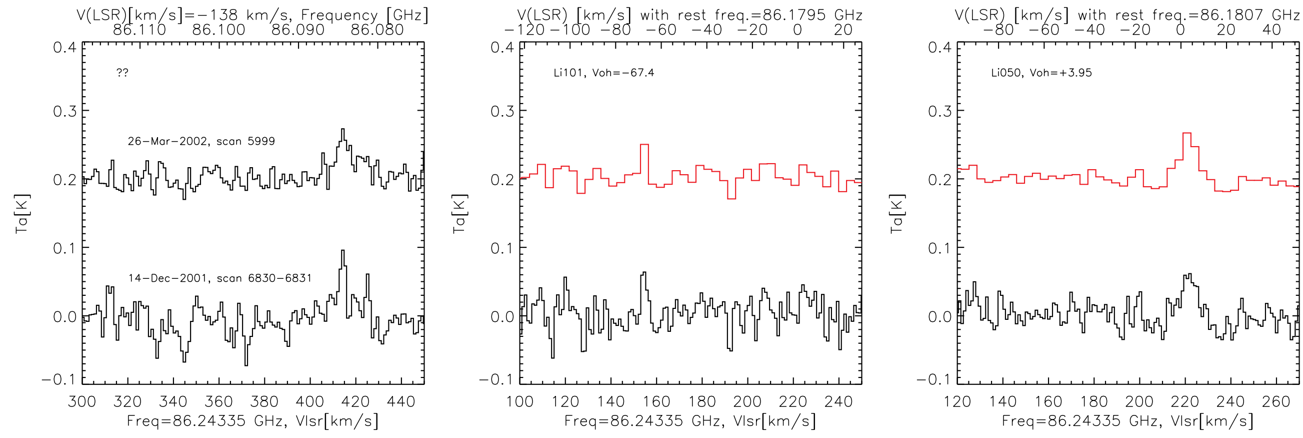

Fig. 2. Left-hand panel: spectra of the high-velocity line in the beam of Li004. Two spectra obtained with the auto-correlator in two different epochs are plotted in black. By assuming it arises from the OH/IR star (OH $V_{\rm LSR} = -138.2\,{\rm km\,s^{-1}}$ at 1612 MHz), the line frequency is estimated on the top axis. Middle and right-hand panels: spectra of a second detection in the beams of Li101 and Li050. By assuming the SiO rest frequency, the new lines are shifted by $\Delta V_{\rm LSR} = 220 \pm 2.8\,{\rm km\,s^{-1}}$ with respect to the OH lines at 1612 MHz. The exact frequencies obtained by assuming the velocities of the OH/IR stars are given in the figure titles. When using the rest frequency of the CCS line (86.181 GHz) we obtain $\Delta V_{\rm LSR} = 217\,{\rm km\,s^{-1}}$, and with the OH molecular transition at 86.178 GHz $\Delta V_{\rm LSR} = 227\,{\rm km\,s^{-1}}$. (Color online)

emission (seen in both epochs). Detections of other transitions are needed to confirm the nature of this line that could arise from the envelope of the highest-velocity AGB star measured in the GC.

4 Available photometric magnitudes

OH/IR stars are among the brightest mid-infrared sources; indeed, a large number of OH/IR stars were already seen with the IRAS mid-infrared satellite. They are easily detected even in the crowded Galactic centre region (Ortiz et al. 2002). The observed OH/IR stars are located within ISOGAL fields and coincide with bright 15-μm point sources (Omont et al. 2003; Schuller et al. 2003; Ortiz et al. 2002). Wood, Habing, and McGregor (1998) was the first to monitor the Galactic centre OH/IR stars photometrically at near-infrared wavelengths and to discover that they mostly coincided with long-period variables. Wood, Habing, and McGregor (1998) provided near-infrared magnitudes of the identified long-period variables (the CASPIR pixel scale was 0.″25). They were found within 2″ from the radio positions of the OH masers. While the mid-infrared measurements of OH/IR stars are unambiguously retrieved, by being the brightest sources of the field, near-infrared counterparts are often too faint to be detected.

In table 3, we revised the mid-infrared measurements of the stars by searching within the Midcourse Space Experiment (MSX) (with a sensitivity in A-band of 0.1 Jy and a maximum flux measured of ≈700 Jy; Egan et al. 2003; Price et al. 2001), The Wide-field Infrared Survey Explorer (WISE) [with a sensitivity of ≈0.9 mJy (3.8 mag) and a saturation at ≈140 Jy (−3.0 mag) at 11.6 μm; Wright et al. (2010) and the WISE All-Sky online catalog], MIPS Galactic Plane Survey (MIPSGAL) (Gutermuth & Heyer 2015), and Galactic Legacy Infrared Midplane Survey Extraordinaire (GLIMPSE) catalogs (with fluxes from ≈10 mJy to 1.6 Jy at at 8 μm in v2; Churchwell et al. 2009; Benjamin et al. 2003). Pointing positions were taken from a preliminary version of the ISOGAL catalog (within 1″; Omont et al. 2003), and are listed in tables 1 and 2. For all pointing positions a unique MSX counterpart was found within a search radius of 14.″5 (the IRAM half beam size). MSX has a spatial resolution of 18.″3 in the A band; the average distances from our positions and the MSX centroids is of 3.″0 with a σ of 2.″2. MSX point sources were not available in correspondence of four OH maser positions. The flux at 8 μm (A band) ranges from ∼0.15 to ∼11.0 Jy, with a mean of 1.6 Jy ($\sigma = 1.4$ Jy).

WISE imaged the sky with a spatial resolution of 6″ and an astrometric accuracy within 0.″4 (Wright et al. 2010). By using a search radius to 10″, we found 64 WISE matches to our 67 OH/IR stars. We searched for the closest GLIMPSE counterparts by adopting a search radius of 10″. To avoid false identifications, knowing that OH/IR stars are among the brightest and reddest mid-infrared point sources (Ortiz et al. 2002), we first considered data points with [8.0] < 7.0 mag. A total of 58 GLIMPSE valid matches to the 67 OH/IR stars were retrieved, plus a match for V4502 Sgr.

Average near-infrared magnitudes were provided by Wood, Habing, and McGregor (1998), Glass et al. (2001), and Matsunaga et al. (2009) for 57 targets and periods for 53 targets (see tables 1, 2, and 3).

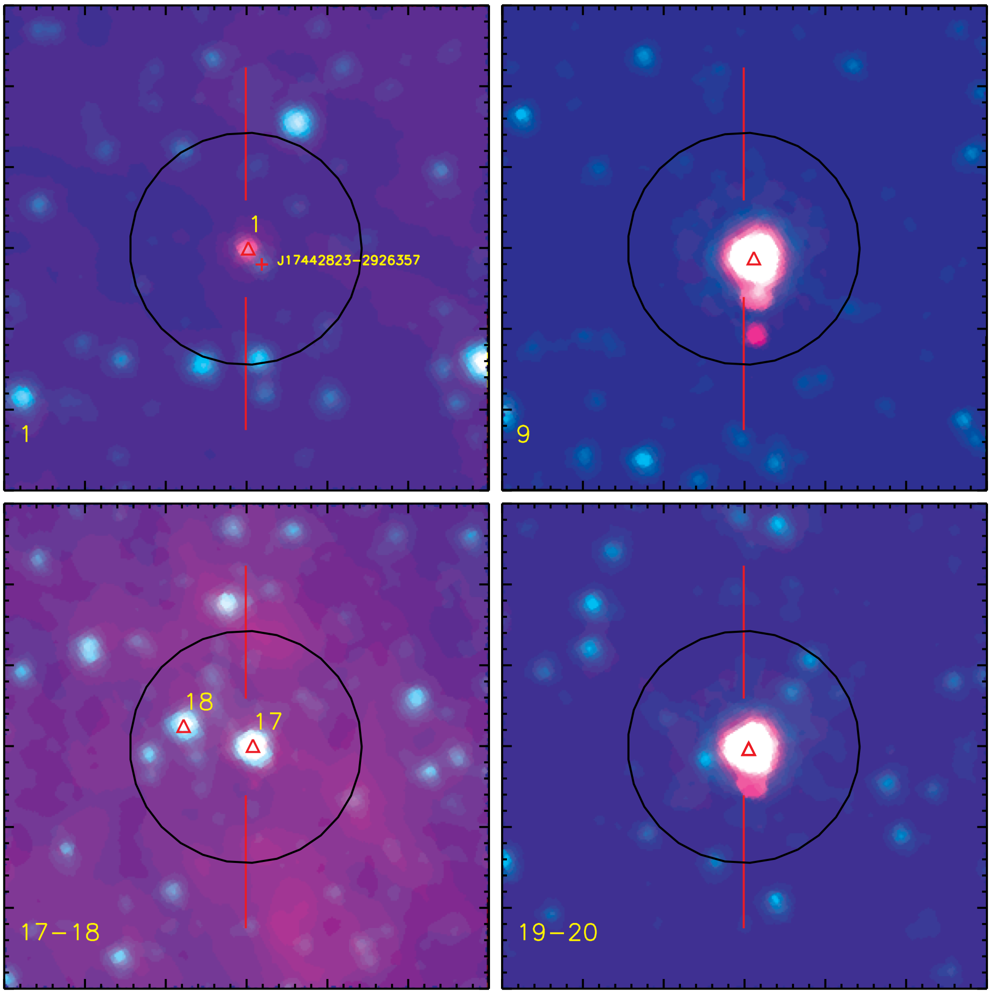

Fig. 3. Composite image. Red shows the GLIMPSE 8 μm image, green the GLIMPSE 4.5 μm, and blue the UKIDSS K-band image. Identification numbers are as in tables 1 and 2 of this paper. North is up and east to the left. The large black circle is centred on the IRAM pointing and has a diameter of 29″. The red triangles mark the targeted OH/IR stars and the V4502 Sgr (ID = 18) variable, clockwise from the upper left, respectively; source ID 1, source ID 9, source IDs 19/20, and source IDs 17/18. The red cross marks the location of 2MASS J17442823−2926357, which is near Li004 (ID = 1) (not detected in the *K* band).

As stated above, near-infrared counterparts have historically been found by detecting long-period variables, but coordinates with a subarcsec accuracy are often missing. Nowadays, with the availability of accurate astrometry from several near-infrared Galactic plane surveys, it is possible to retrieve them by positional coincidence. We retrieved the original near-infrared 2MASS coordinates (JHK_s; Skrutskie et al. 2006) of the matches provided by WISE and GLIMPSE. In highly-crowded regions at the resolution of GLIMPSE near-infrared misidentification are possible, especially for the faintest stars. We checked the 2MASS positions and GLIMPSE positions with the source centroids of the GLIMPSE 8-μm and UKIDSS K-band charts. UKIDSS images have a spatial resolution of 0.″2 (Lucas et al. 2008). GLIMPSE coordinates had to be astrometrically improved only for stars #33, #46, #55, #66, #68, by taking the UKIDSS data point coinciding with the GLIMPSE centroid in order to avoid misidentification.

With the improved coordinates, we searched in the General Catalogue of Variable Stars (GCVS) (Samus' et al. 2017). 47 of the 67 OH/IR stars were identified within a search radius of 1″, plus two other secure identifications were made at a larger separation (see table 3 footnotes). One of the near-infrared counterparts identified by Wood, Habing, and McGregor (1998) appeared incorrect (see the details on star #1 in the subsection 4.1).

For most of these stars the stellar spectral energy distribution, based on average near-infrared magnitudes plus several mid-infrared bands, was analysed by Wood, Habing, and McGregor (1998) and Ortiz et al. (2002), and estimates of extinction and bolometric fluxes are provided in their works. Furthermore, the near-infrared spectra taken by Vanhollebeke et al. (2006) confirm strong water

Table 3. Infrared measurements of the targeted OH/IR stars and of the serendipitous detection of V4502 Sgr.*

	NIR positions				Averages			GCVS*		ISOGAL		GLIMPSE†				MSX†				WISE†				MIPSGAL
ID	RA	Dec	Survey	2MASS K_s [mag]	⟨*J*⟩ [mag]	⟨*H*⟩ [mag]	⟨*K*⟩ [mag]	Sep [″]	GCVS	[7] [mag]	[15] [″]	[3.6] [mag]	[4.5] [mag]	[5.8] [mag]	[8.0] [mag]	*A* [mag]	*C* [mag]	*D* [mag]	*E* [mag]	*W1* [mag]	*W2* [mag]	*W3* [mag]	*W4* [mag]	24 μm [mag]
1	17 44 28.37	−29 26 33.71	GLIMPSE	..	..	13.60?	11.48?	..	none	6.53	4.24	..	10.37	7.80	6.11	5.71	98.98	3.92	98.98	..	..	..	..	2.42
2	17 44 34.96	−29 04 35.67	2MASS	9.24	..	..	..	0.0	V4458 Sgr	1.30	−0.48	88.88	88.88	88.88	88.88	1.83	0.52	−0.05	−0.83	6.07	3.19	1.58	−0.29	..
3	17 44 39.67	−29 16 46.38	2MASS	11.03	..	..	10.87	0.1	V4462 Sgr	4.50	2.35	7.16	6.05	4.47	4.13	3.94	2.85	2.26	1.67	7.63	5.01	3.25	1.47	1.90
4	17 44 45.96	−29 06 13.63	2MASS	11.22	..	14.34	10.66	0.0	V4465 Sgr	3.17	2.37	6.69	4.81	3.73	3.04	3.83	2.71	1.95	1.36	7.09	4.92	3.04	1.12	1.07
5	17 44 51.25	−29 09 45.31	2MASS	11.21	..	..	11.46	0.0	V4466 Sgr	4.44	2.85	7.76	6.39	5.28	4.69	4.30	3.26	2.74	2.29	8.54	6.43	4.70	1.65	2.03
6	17 44 56.83	−29 13 25.51	2MASS	7.77	..	..	..	0.0	V4470 Sgr	3.14	2.06	5.33	4.61	3.93	3.24	3.54	2.33	1.78	1.03	5.92	3.68	2.47	0.28	1.41
7	17 45 03.20	−29 07 12.64	2MASS	10.42	..	12.85	9.71	0.0	V4473 Sgr	4.83	3.53	6.61	..	4.27	4.18	..	..	..	..	4.41	4.84	3.29	1.62	2.29
8	17 45 05.29	−29 17 13.42	2MASS	6.88	12.03	9.11	7.41	0.1	V4475 Sgr	4.21	2.73	88.88	88.88	88.88	88.88	3.91	2.69	2.23	0.38	6.34	5.52	3.20	−0.05	..
9	17 45 11.45	−28 38 38.53	2MASS	11.27	..	..	11.85	0.1	V4481 Sgr	3.44	1.41	6.69	4.71	3.73	3.01	3.33	2.12	1.46	0.84	7.34	4.93	3.08	1.05	1.19
10	17 45 12.92	−29 12 54.67	2MASS	9.67	..	12.98	9.68	0.1	V4482 Sgr	3.49	2.66	..	..	..	..	3.61	2.32	1.96	1.48	6.30	4.27	2.73	1.24	1.09
11	17 45 13.91	−28 47 43.20	2MASS	10.57	..	13.85	10.34	0.1	V4489 Sgr	3.43	1.43	..	..	..	..	3.59	2.40	1.82	1.27	6.54	4.28	2.49	0.66	1.01
12	17 45 13.88	−29 06 55.40	GLIMPSE	..	..	..	13.48	..	none	3.35	2.23	9.55	7.18	5.32	4.32	3.40	2.41	1.56	1.23	9.03	6.54	3.48	1.44	..
13	17 45 14.27	−29 07 20.75	2MASS	11.13	..	14.54	11.14	0.1	V4487 Sgr	4.14	2.40	..	..	..	..	4.45	3.11	2.65	2.84	7.76	6.00	4.19	2.66	2.33
14	17 45 17.83	−29 05 53.34	2MASS	10.57	..	14.25	10.46	0.0	V4492 Sgr	4.19	2.91	7.77	6.58	5.39	4.50	4.17	3.12	2.43	1.68	8.16	5.69	3.25	0.64	1.07
15	17 45 19.34	−29 14 05.79	2MASS	8.48	..	12.25	8.97	0.0	V4494 Sgr	4.08	2.02	5.27	4.71	3.88	3.31	3.60	2.44	2.03	1.43	6.05	4.14	2.52	0.74	1.78
16	17 45 29.42	−28 39 34.96	2MASS	10.80	..	13.51	10.63	0.1	V4499 Sgr	4.55	2.50	6.88	6.12	4.48	4.00	3.83	2.64	2.02	1.55	6.29	4.22	2.41	0.75	0.85
17	17 45 31.43	−28 46 21.89	2MASS	8.96	14.46	10.88	..	0.3	V4501 Sgr	4.87	3.60	7.13	6.49	5.87	5.47	97.97	97.97	97.97	98.98	..	..	..	..	..
18	17 45 32.09	−28 46 19.42	2MASS	8.57	..	..	..	0.0	V4502 Sgr	..	..	7.28	7.10	6.61	6.65	97.97	97.97	97.97	98.98	..	..	..	..	..
19	17 45 34.79	−29 06 02.68	2MASS	8.98	15.91	11.47	9.05	0.1	V4507 Sgr	3.56	2.55	5.59	4.75	3.90	3.25	3.90	2.69	2.18	2.08	6.06	4.31	2.87	1.03	..
20	17 45 34.79	−29 06 02.68	2MASS	8.98	15.91	11.47	9.05	0.1	V4507 Sgr	3.56	2.55	5.59	4.75	3.90	3.25	3.90	2.69	2.18	2.08	6.06	4.31	2.87	1.03	..
21	17 45 48.48	−29 10 45.20	2MASS	9.74	..	12.58	9.57	0.0	V4519 Sgr	4.90	3.52	6.63	5.82	4.34	4.11	4.61	3.40	2.96	2.52	7.63	5.72	3.93	2.27	2.01
22	17 45 56.08	−28 39 27.46	2MASS	9.79	..	..	10.48	0.1	V4532 Sgr	..	1.88	6.84	6.16	4.63	4.20	3.40	2.08	1.72	1.19	5.87	3.93	2.49	0.58	1.02
23	17 46 14.96	−28 44 17.34	2MASS	9.24	15.35	11.02	8.76	0.0	V4549 Sgr	4.56	3.07	6.77	6.28	5.03	4.72	4.63	3.27	2.49	0.81	7.39	5.98	3.81	0.31	..
24	17 46 19.51	−29 00 41.34	2MASS	10.63	..	..	11.68	..	none	4.89	2.58	7.72	6.34	5.11	4.41	5.20	3.89	2.75	1.54	7.08	4.77	3.09	0.72	..
25	17 46 22.11	−28 46 22.61	2MASS	9.19	..	13.14	9.93	0.0	V4551 Sgr	3.84	1.97	6.84	5.99	4.40	4.07	3.77	2.55	2.00	0.86	7.18	5.76	4.61	−2.13	..
26	17 46 28.71	−28 53 19.49	2MASS	8.15	15.67	11.48	8.85	0.0	V4555 Sgr	4.54	2.64	6.67	5.56	4.62	4.17	4.64	3.18	2.87	2.76	6.48	5.07	3.48	1.61	1.45
27	17 46 31.23	−28 39 48.68	2MASS	8.26	..	11.62	8.84	..	none	4.86	3.09	6.68	6.20	5.05	4.71	4.12	2.67	2.35	0.81	7.33	6.23	5.09	98.98	2.01
28	17 46 33.07	−28 45 01.04	2MASS	10.08	..	..	10.49	..	none	4.89	4.04	7.12	6.18	4.86	4.55	..	..	..	..	..	..	..	..	2.94
29	17 46 38.51	−29 08 01.22	GLIMPSE	95.95	..	..	..	..	none	4.66	2.64	7.27	6.10	5.04	4.42	4.56	3.27	2.80	2.62	6.66	4.93	3.25	1.40	2.00
30	17 47 02.17	−28 45 55.79	2MASS	8.78	..	13.10	9.94	0.0	V4570 Sgr	4.32	2.88	7.04	6.28	5.08	4.50	5.14	3.69	3.09	98.98	7.34	5.76	4.12	1.88	1.20
31	17 47 21.28	−28 39 22.84	2MASS	10.74	..	..	11.52	0.1	V4573 Sgr	3.64	1.88	7.63	6.30	5.09	4.45	3.59	2.36	1.79	1.28	6.67	4.59	2.96	0.97	0.95
32	17 47 24.02	−28 32 42.93	2MASS	8.14	..	11.99	8.80	0.1	V4574 Sgr	3.48	2.12	5.62	4.55	3.82	3.24	3.48	2.29	1.84	1.42	7.16	5.39	3.58	1.49	1.90
33	17 43 45.48	−29 26 17.22	UKIDSS	95.95	..	..	..	..	none	4.06	2.14	..	7.24	5.03	4.09	4.47	3.04	1.97	1.44	9.52	6.44	2.77	0.66	..
34	17 43 53.95	−29 25 23.43	GLIMPSE	95.95	..	..	..	..	none	4.48	1.80	7.53	6.07	3.94	3.09	4.37	3.38	2.25	1.49	8.19	4.92	2.47	0.27	1.08
35	17 44 14.95	−28 45 06.02	2MASS	8.49	13.86	10.31	8.13	0.1	V4449 Sgr	4.24	1.95	6.70	6.17	4.77	4.10	3.80	2.43	2.15	1.16	6.82	5.77	3.99	1.94	1.89
36	17 44 34.48	−29 10 37.23	GLIMPSE	95.95	..	..	11.21	..	none	4.05	1.76	7.20	5.16	4.67	..	3.95	2.84	2.03	1.45	6.95	5.07	3.06	0.77	1.02
37	17 44 44.43	−29 05 37.92	2MASS	9.92	..	14.00	10.40	0.0	V4463 Sgr	3.57	2.05	7.44	6.32	5.18	4.56	3.77	2.61	1.91	1.39	7.19	5.00	2.98	1.08	1.10
38	17 44 47.94	−29 06 49.93	2MASS	9.39	14.92	11.28	9.43	..	none	5.03	2.85	7.81	7.20	5.73	4.71	4.81	3.62	2.55	2.23	7.64	6.45	4.09	1.90	1.48
39	17 44 54.16	−29 13 44.88	2MASS	8.52	15.53	11.07	8.67	0.0	V4468 Sgr	4.89	3.23	88.88	88.88	88.88	88.88	3.78	2.28	1.71	−0.13	6.89	6.08	4.09	1.65	..
40	17 44 57.74	−29 20 42.42	2MASS	11.91	..	..	10.85	0.1	V4471 Sgr	4.66	2.45	6.75	5.92	4.12	3.46	4.34	3.03	2.31	1.06	8.66	6.36	4.05	0.30	..
41	17 45 01.70	−29 02 49.90	2MASS	8.54	13.47	10.26	8.28	0.0	V4779 Sgr	4.91	3.26	6.69	6.13	5.10	4.57	4.22	2.89	2.70	2.26	6.35	5.08	3.56	1.65	2.21
42	17 45 06.90	−29 03 33.40	GLIMPSE	95.95	14.64	11.11	9.04	..	none	4.86	2.73	7.15	6.45	5.77	5.22	5.08	3.24	2.39	1.02	6.52	5.09	3.24	0.34	..
43	17 45 10.39	−29 18 12.26	2MASS	12.65	..	14.80	11.11	0.1	V4480 Sgr	3.98	1.80	7.84	6.76	4.92	4.23	4.38	3.34	2.49	1.59	7.28	4.48	2.67	0.43	..
44	17 45 12.45	−28 40 44.39	2MASS	9.80	..	11.47	8.69	0.0	V4484 Sgr	4.68	1.36	7.72	6.40	5.16	4.18	3.57	2.24	1.78	0.97	8.73	6.84	3.71	1.50	1.37
45	17 45 13.07	−29 09 36.33	2MASS	9.72	15.35	11.51	9.38	0.0	V4483 Sgr	4.29	2.83	6.82	5.70	4.99	4.46	4.34	3.27	2.72	2.06	6.44	5.04	4.44	3.17	2.46

Table 3. (Continued)

ID	NIR positions				Averages			GCVS*		ISOGAL		GLIMPSE†				MSX†				WISE†				MIPSGAL
	RA	Dec	Survey	2MASS K_s [mag]	⟨J⟩ [mag]	⟨H⟩ [mag]	⟨K⟩ [mag]	Sep [″]	GCVS	[7] [mag]	[15] [″]	[3.6] [mag]	[4.5] [mag]	[5.8] [mag]	[8.0] [mag]	A [mag]	C [mag]	D [mag]	E [mag]	W1 [mag]	W2 [mag]	W3 [mag]	W4 [mag]	24 μm [mag]
46	17 45 13.86	−29 15 28.73	UKIDSS	95.95	..	..	11.25	2.1	V4485 Sgr[a]	3.47	1.59	..	..	..	..	3.24	2.11	1.50	0.33	6.65	3.97	2.52	−0.68	..
47	17 45 16.43	−29 15 37.61	2MASS	7.66	14.26	10.54	8.42	0.0	V4490 Sgr	4.60	3.48	6.68	6.13	5.06	4.74	3.79	2.61	2.44	1.00	6.33	5.18	3.27	0.63	..
48	17 45 18.04	−29 18 03.91	GLIMPSE	95.95	..	..	13.67	0.5	V4491 Sgr	5.91	4.32	8.67	6.46	5.41	4.99	6.61	98.98	4.73	98.98	10.47	6.54	5.61	3.14	3.50
49	17 45 29.24	−29 07 04.25	2MASS	9.54	..	12.70	10.09	0.1	V4875 Sgr	4.40	2.96	7.32	6.55	5.65	5.20	4.67	3.33	2.96	2.13	6.84	5.79	4.19	1.64	1.96
50	17 45 29.46	−29 09 16.42	GLIMPSE	..	..	..	11.41	..	none	4.87	3.06	7.82	6.67	5.49	4.95	4.78	3.90	3.22	2.57	8.46	6.27	4.41	1.61	1.44
51	17 45 33.26	−29 11 23.20	GLIMPSE	..	..	..	12.54	..	none	5.34	3.81	9.75	7.58	6.22	5.54	..	..	..	..	98.98	6.81	4.87	2.53	3.24
52	17 45 33.44	−28 43 45.00	2MASS	10.83	..	..	10.78	..	none	4.00	2.07	6.88	5.82	4.26	4.05	3.79	2.52	2.18	1.54	6.67	5.17	2.64	0.68	1.83
53	17 45 34.41	−29 12 54.12	2MASS	9.93	..	..	..	..	none	4.30	2.71	6.85	6.38	4.87	4.43	5.30	3.79	3.08	2.42	6.23	4.49	3.09	1.30	2.06
54	17 45 46.57	−28 32 39.50	2MASS	10.35	..	13.43	9.36	0.0	V4518 Sgr	3.36	1.73	..	..	..	..	3.64	2.50	2.00	1.37	7.32	5.32	3.47	1.29	1.33
55	17 45 54.21	−28 31 47.06	UKIDSS	11.49	..	..	9.62	1.1	V4529 Sgr[b]	3.85	1.66	88.88	88.88	88.88	88.88	3.25	2.04	1.25	0.92	7.48	5.11	2.97	0.84	..
56	17 46 00.92	−29 01 23.24	GLIMPSE	..	..	..	14.79	0.3	V4538 Sgr	2.30	0.59	7.00	4.59	2.63	..	3.75	2.50	1.63	1.08	9.04	5.44	2.17	0.11	..
57	17 46 11.68	−28 59 32.44	2MASS	9.40	..	13.20	9.58	0.0	V5020 Sgr	5.23	3.87	7.16	6.37	5.42	4.89	4.93	3.92	3.12	2.22	7.56	5.87	3.72	0.37	2.53
58	17 46 14.48	−28 36 39.54	2MASS	12.02	..	..	12.62	0.1	V4548 Sgr	4.28	3.29	8.81	7.16	5.90	5.24	4.40	3.38	2.90	2.53	7.94	5.72	4.18	2.13	2.29
59	17 46 15.25	−28 55 42.36	GLIMPSE	..	..	..	..	0.1	V4550 Sgr	3.24	1.55	9.20	6.98	5.31	4.42	3.67	2.52	1.65	1.16	8.55	5.49	3.01	0.14	..
60	17 46 15.74	−28 56 32.27	2MASS	10.09	..	14.03	10.05	0.0	V5039 Sgr	5.30	3.31	7.15	6.04	4.87	4.33	4.99	3.61	2.68	1.46	7.81	5.93	3.97	0.64	..
61	17 46 24.87	−29 00 01.41	2MASS	10.97	..	15.22	11.21	0.0	V4552 Sgr	4.72	2.80	7.70	6.40	5.27	4.70	4.62	3.40	2.59	2.02	7.00	4.84	3.42	0.63	1.25
62	17 46 30.71	−28 31 32.81	GLIMPSE	95.95	..	12.47	9.65	..	none	7.03	5.77	8.22	7.13	6.79	6.70	..	..	..	..	8.25	7.20	6.37	3.48	4.16
63	17 46 31.68	−28 35 41.05	GLIMPSE	95.95	..	14.83	11.60	0.3	V4559 Sgr	4.56	3.11	7.90	6.39	5.35	4.86	4.84	3.73	3.28	98.98	6.47	5.97	5.19	1.73	2.33
64	17 46 35.31	−28 58 57.05	GLIMPSE	..	..	..	..	0.2	V4562 Sgr	4.26	2.26	8.16	6.18	4.13	3.11	3.43	2.24	1.50	0.74	9.10	6.47	2.90	0.31	1.45
65	17 46 42.29	−28 33 26.13	2MASS	11.41	..	14.97	11.18	0.0	V4567 Sgr	4.74	3.98	7.91	6.39	5.42	5.03	5.15	98.98	4.14	98.98	8.66	6.73	5.00	1.68	3.42
66	17 46 44.84	−28 34 59.66	UKIDSS	95.95	..	..	..	..	none	4.70	2.49	8.08	6.35	4.89	4.22	4.54	3.34	2.87	2.87	7.83	5.09	3.21	1.38	1.20
67	17 46 47.81	−28 47 15.16	GLIMPSE	..	..	..	13.62	0.3	V4568 Sgr	5.72	3.50	9.90	8.14	6.59	5.55	5.49	3.95	3.42	3.07	10.60	7.95	4.52	1.25	2.61
68	17 46 58.95	−28 17 00.56	UKIDSS	95.95	..	..	..	..	none	4.06	1.67	8.37	6.27	4.77	4.03	3.65	2.29	1.75	0.99	8.27	5.14	2.87	0.66	..
69	17 47 39.65	−28 35 46.78	GLIMPSE	..	..	..	13.47	0.8	V4575 Sgr	..	2.20	6.71	4.76	3.65	..	2.86	1.86	1.13	0.54	6.95	3.69	1.98	0.18	0.99

*Notes: *a*—Star #46 coincides (0.″05) with V4485 Sgr (Hmag =14.299 mag, Ksmag =10.714 mag and ΔK =2.030 mag) which is analyzed in the VVV catalog of Galactic Bulge Type II Cepheids NIR data by Braga et al. (2019) (note that the GCVS has the old coordinates, 2.″1 away). *b*—The 2MASS centroid of star #55 was recentered. This star coincides with V4529 Sgr (note that the GCVS has the old coordinate, 1.″1 away).

†Magic values: ..—Not available. 88.88—Retrieved match false, star not extracted, image saturation. 95.95—2MASS (provided by WISE or GLIMPSE) or ISOGAL-DENIS data points were false near-infrared matches and removed. 97.97—Confusion. 98.98—Upper limit.

vapour absorption, which is the typical signature of large-amplitude AGB variables.

4.1 Serendipitous 86-GHz detections: ID = #1, #9, #18, and #20

For positions with two 86-GHz lines detected (Li091 and Li050) and with 86-GHz lines at significantly different velocities than that of the known OH masers (Li004 and Li101), we carefully inspected the GLIMPSE and UKIDSS images. Maser emitters are usually associated with bright mid-infrared data points (see figure 3).

At the position of the OH/IR star Li004 (ID = #1), which is not seen at 86 GHz, a line is detected at 415 $\mathrm{km\,s^{-1}}$. Li004 is the brightest mid-infrared star with [4.5] = 10.4 mag, [5.8] = 7.8 mag, and [8.0] = 6.11 mag, [15.0] = 4.24 mag. At this location no UKIDSS data point is seen, and the GLIMPSE images show a nearby peak at a small separation of $\approx 2\farcs5$ with [3.6] = 9.969 mag, [4.5] = 9.730 mag, [5.8] = 9.444 mag (not detected at 8 μm). The ISOGAL/DENIS ($K_s = 11.5$ mag) position coincides with this other source seen at 3.6 μm (which is not centred on the 8-μm source) and with the 2MASS J17442823−2926357 (K_s = 11.5 mag), UKIDSS K-band data point (UGPS J174428.23–292635.7, $K = 11.43$ mag). Wood, Habing, and McGregor (1998) did not detect any variability and reported an average $K = 11.48$ mag, i.e., they analysed 2MASS J17442823–2926357, a false counterpart to the OH/IR stars. Only two other 8-μm GLIMPSE stars fall within the IRAM beam. They are faint with [8.0] = 7.70 and 7.80 mag ($K_s = 9.75$ and 10.61 mag).

With an $8\farcs8$ separation between Li091 (ID = 17) and V4502Sgr (ID = 18), both stars fall within the IRAM beam. Li091, which is the OH/IR star, coincides with the bright 15-μm star detected by ISOGAL (3.6 mag; Ortiz et al. 2002). Both variables are detected by GLIMPSE with [8.0] = 5.47 and 6.65 mag, and [3.6−8.0] = 1.66 and 0.63 mag, respectively.

A second 86-GHz line is detected at the position of Li050 (lines ID = #19 and #20), and a line at an unexpected velocity is found in the direction of Li101 (ID = #9). There are no other bright mid-infrared stars ([8.0] < 8.9 mag) in these positions. The sources were not observed by Stroh et al. (2019) (M. C. Stroh 2020 private communication). There are no other reports of these line detections towards these sources.

5 SiO masers and properties of the OH/IR stars

A global detection rate of 42% is obtained for 86-GHz SiO masers in OH/IR stars.

5.1 SiO maser detections and MSX colors: difference between Miras and OH/IR stars.

OH/IR stars are the most obscured long-period variables, with optically thick envelopes, as already inferred from studies of the mid-infrared colors from IRAS (Habing 1996).

In our 2000–2003 search for 86-GHz maser emission (Messineo 2004), we deliberately selected Mira-like stars and excluded OH/IR-like stars by targeting bluer colors (Messineo et al. 2002). There were several reasons to do so; efficiency in increasing the number of stellar velocities in a manner complementary to OH surveys, and previous knowledge [at that time provided by, e.g., Haikala, Nyman, and Forsstroem (1994) and Bujarrabal (1994)] that 86-GHz maser emission was more frequently detected in Mira stars than in thicker-shelled OH/IR stars. With the presented dataset we can verify our hypothesis, which was based on a very small number of sources, and possibly even determine a change in the detection rate of SiO masers with stellar colors.

Mira-like stars have a color distribution indistinguishable from that of the OH/IR stars in the ($D - E$) versus ($A - C$) diagram (see figures in Messineo et al. 2018). This diagram is useful only to separate mass-loss AGB stars from post-AGBs (Sevenster 2002). There is another combination of MSX filters that allows us to separate Mira-like AGB stars with thinner envelopes from the thicker-envelope OH/IR stars (Messineo et al. 2004; Lumsden et al. 2002). In figure 4, we show the MSX $C - D$ versus $A - E$ colors.[3]

The OH/IR stars appear to have redder $C - D$ colors and $A - E$ colors than the comparison sample of Mira-like stars (without OH emission) from Messineo's thesis (Messineo et al. 2004, 2018). The colors are not corrected for interstellar extinction, however, for $A_{K_s} = 3$ mag the corrections to the $C - D$ colors are within 0.3–0.6 mag and those made to the $A - E$ colors are within 0.3–0.4 mag (Messineo et al. 2005). The bulk of Mira-like stars from Messineo et al. (2018) (see also Messineo et al. 2002) have $A - E$ colors from 1.0 to 2.5 mag, while the OH/IR stars studied here have redder $A - E$ colors from 1.5 to 4.0 mag. For the Mira-like stars of Messineo et al. (2018), the SiO detection rate is 66% (261 targets and 172 detections) for colors $A - E < 2.5$ mag, but is equal to 43% when considering the remaining Mira-like stars (21 targets and nine detections) with $2.5 < A - E < 3.5$ mag. For the 29 OH/IR stars with $A - E < 2.5$ mag (average $C - D = 0.54$ mag, $\sigma = 0.16$ mag), the 86-GHz SiO detection rate is 59%, similar to that of the Mira-like stars. For the 28 OH/IR stars with

[3] C, D, A, and E indicated the MSX magnitudes. The A band covers from 6 to 11 μm, the C-band from 11 to 13 μm, the D-band covers from 13.5 to 16 μm, and the E-band covers from 18 to 25 μm, as shown in figure 1 of Messineo et al. (2005).

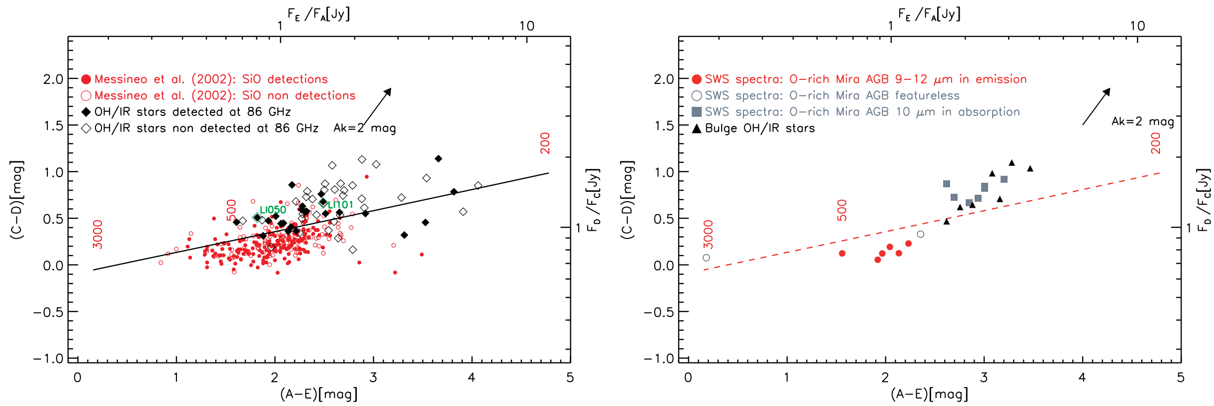

Fig. 4. Left-hand panel: MSX ($C - D$) versus ($A - E$) colors. Black diamonds mark the OH/IR stars analysed in this work (the locations of Li101 and Li050 are marked in green with two green labels), while red circles mark the Mira-like stars of Messineo et al. (2002). 86-GHz SiO maser detections are marked with filled symbols, non-detections with open symbols. Right-hand panel: MSX $C - D$ versus $A - E$ plot of O-rich Mira stars with ISO-SWS spectra. Red-filled circles mark those ISO-SWS spectra with 10-μm silicate features in emission, while gray-filled squares indicate those with the silicate feature in absorption. For comparison, the seven bulge OH/IR stars modeled in Blommaert et al. (2018) (with silicate features in absorption) are plotted with black-filled triangles. (Color online)

$A - E > 2.5$ mag (with average $C - D = 0.70$ mag, $\sigma = 0.26$ mag), the 86-GHz detection rate is 25%. The 86-GHz SiO detection rate drops for sources redder than $A - E = 2.5$ mag. This is somewhat in line with the earlier findings of Haikala, Nyman, and Forsstroem (1994) and Bujarrabal (1994) that 86-GHz maser emission occurs more frequently in Miras than in OH/IR stars. They must have looked at the reddest OH/IR stars.

The redder $C - D$ colors of the OH/IR stars are most likely due to the broad 10 μm silicate features (in absorption from ≈8 to ≈12.5 μm) in combination with the MSX filter profiles (Messineo et al. 2004). In figure 4, we also plot the MSX colors of O-rich Miras and OH/IR stars with ISO-SWS spectra available from the library of Sloan et al. (2003). O-rich Miras with 10 μm silicate spectra in emission have $C - D$ colors located below the blackbody curve, as expected by Messineo et al. (2004). The $C - D$ colors of stars with a 10 μm feature in absorption fall above the curve. For comparison, the MSX colors of the bulge OH/IR stars modeled by Blommaert et al. (2018) are shown, and they also fall above the blackbody line.

Most of the sources here considered have $D - E < 1.38$ mag, which delimits the color region dominated by SiO masers described in Stroh et al. (2019) (with an SiO detection rate of 80% at the high sensitivity of ALMA). Indeed, 99% of the Mira-like stars in Messineo et al. (2018) have colours $D - E < 1.38$ mag and 91% of the OH/IR stars here studied (among the five redder OH/IR stars there are three SiO maser detections).

The bluer Mira-like stars detected at 86 GHz have mass-loss rates from 10^{-7} to $2 \times 10^{-5}\,M_\odot\,\mathrm{yr}^{-1}$ with a peak at 10^{-6}–$10^{-5} M_\odot\,\mathrm{yr}^{-1}$ (Messineo et al. 2004). For bulge OH/IR stars, Ortiz et al. (2002) estimate mass-loss rates from 3×10^{-6} to a few $10^{-5}\,M_\odot\,\mathrm{yr}^{-1}$. The rare (seven) CO line detections in bulge OH/IR stars yield estimates of mass-loss rates from 2×10^{-5} to $9.5 \times 10^{-5}\,M_\odot\,\mathrm{yr}^{-1}$ (Blommaert et al. 2018).

5.2 Line ratios

We searched the literature for previous detections of these SiO masers at 43 GHz (e.g., Deguchi et al. 2000a, 2000b, 2004; Li et al. 2010; Fujii et al. 2006; Sjouwerman et al. 2002; Izumiura et al. 1998; Shiki & Deguchi 1997; Lindqvist et al. 1991). We found detections for only 22 of the OH/IR stars and non-detections for four of the OH/IR stars. There are 10 detections at both 86 and 43 GHz which yield these average ratios $I(43\mathrm{GHz},v = 1)/I(86\mathrm{GHz},v = 1) = 1.09$ and $I(43\mathrm{GHz},v = 2)/I(86\mathrm{GHz},v = 1) = 1.75$. Despite the non simultaneity of the data, taken at a random phase, the mean is meaningful because the photometric variations of the stars are not synchronised one to another. These values are similar to the quasi-simultaneous ratios analyzed by Stroh et al. (2018) for a selection of thinner-shell Miras.

5.3 SiO detection rates and periods, V_{exp}, Mbol: difference between Miras and OH/IR stars

We analyzed the 86-GHz detections as a function of the stellar periods and amplitudes (see tables 1 and 2). Interestingly, it appears that 86-GHz SiO maser detections arise from OH/IR stars with periods longer than 500 days. By restricting the analysis to periods >500 days, the 86-GHz detection rate increases to 57% (the global detection rate is 42%). That the SiO maser detection rate is a steep function of periods had already been concluded from the sample of Galactic centre large-amplitude variables of Glass et al. (2001) and the 43-GHz SiO maser observations of Imai et al. (2002). Thereby, SiO maser emission traces AGB variables with periods longer than 500 days.

All but one of the 86-GHz SiO maser detections belong to OH/IR stars with $V_{exp} > 14.5\,\mathrm{km\,s^{-1}}$. The OH/IR stars V_{exp} are known to increase with stellar periods (Lindqvist et al. 1992).

During their life, long-period variable stars lose mass at increasing rates, thicken their envelopes, and lengthen their periods (Vassiliadis & Wood 1993). Periods depend on the stellar initial masses and ages of the variables. The bulk of the bulge OH/IR stars is made of stars, with M_{bol} from -4.5 to $-5.0\,M_{bol}$ (Ortiz et al. 2002; Blommaert et al. 2018). This M_{bol} range suggests that most of the stars have initial masses between 1.5 and 2 $M_{\odot}$. Because of this relatively narrow range in mass, the variety of observed stellar properties are dominated by evolution rather than initial masses (Ortiz et al. 2002; Blommaert et al. 2018; Qiao et al. 2018). Bulge OH/IR stars do not follow the period–luminosity relation found for bulge Mira stars by Glass et al. (1995), but they are systematically located below it. The commonly accepted interpretation is that, during the pulsating phase, Miras enter a regime of high mass loss (superwind phase) where the AGBs significantly stretch their stellar periods at an almost constant bolometric magnitude (Vassiliadis & Wood 1993), departing from the locus of the Mira period–luminosity relation. OH/IR stars have longer periods for a given luminosity than those found in Mira stars. Of the sampled sources, 43 stars have M_{bol} estimates from the works of Ortiz et al. (2002) and Wood, Habing, and McGregor (1998). They range from -1.99 to -6.35 mag, 20 detections and 23 non-detections. SiO maser detections occur towards stars brighter than $M_{bol} = -3.5$ mag.

Alternatively, Urago et al. (2020) explains these deviations from the period–luminosity relation at 3 μm as attributed to circumstellar extinction. This strengthens the idea of Sjouwerman et al. (2009) that the optical thickness is the key parameter in studying OH/IR stars.

Acknowledgments

IRAM is supported by INSU/CNRS (France), MPG (Germany) and IGN (Spain). MM carried part of this work at the Leiden University in 2001–2002. The work of MM from 2000 to 2004 was funded by the Netherlands Research School for Astronomy (NOVA) through a netwerk 2, Ph.D. stipend. This work was partially supported by the National Natural Science Foundation of China (NSFC-11421303, 11773025), and USTC grant KY2030000054. The National Radio Astronomy Observatory is a facility of the National Science Foundation operated under cooperative agreement by Associated Universities, Inc.

This publication makes use of data products from the Two Micron All Sky Survey, which is a joint project of the University of Massachusetts and the Infrared Processing and Analysis Center/California Institute of Technology, funded by the National Aeronautics and Space Administration and the National Science Foundation. This work is based [in part] on observations made with the Spitzer Space Telescope, which is operated by the Jet Propulsion Laboratory, California Institute of Technology under a contract with NASA. The DENIS project was supported, in France by the Institut National des Sciences de l'Univers, the Education Ministry and the Centre National de la Recherche Scientifique, in Germany by the State of Baden-Wuertemberg, in Spain by the DGICYT, in Italy by the Consiglio Nazionale delle Ricerche, in Austria by the Fonds zur Foerderung der wissenschaftlichen Forschung and the Bundesministerium fuer Wissenschaft und Forschung. This research made use of data products from the Midcourse Space Experiment, the processing of which was funded by the Ballistic Missile Defence Organization with additional support from the NASA office of Space Science. This publication makes use of data products from WISE, which is a joint project of the University of California, Los Angeles, and the Jet Propulsion Laboratory/California Institute of Technology, funded by the National Aeronautics and Space Administration. This work is based on data obtained as part ofthe UKIRT Infrared Deep Sky Survey. Based on observations with ISO, an ESA project with instruments funded by ESA Member States (especially the PI countries: France, Germany, the Netherlands and the United Kingdom) and with the participation of ISAS and NASA. This research has made use of the SIMBAD data base, operated at CDS, Strasbourg, France. This research made use of Montage, funded by the National Aeronautics and Space Administration's Earth Science Technology Office, Computational Technnologies Project, under Cooperative Agreement Number NCC5-626 between NASA and the California Institute of Technology. The code is maintained by the NASA/IPAC Infrared Science Archive. This research hasmade use of NASAs Astrophysics Data System BibliographicServices. The author are grateful to the kind referee for his careful reading and constructive suggestions.

References

Benjamin, R. A., et al. 2003, PASP, 115, 953
Blommaert, J. A. D. L., Groenewegen, M. A. T., Justtanont, K., & Decin, L. 2018, MNRAS, 479, 3545
Braga, V. F., Contreras Ramos, R., Minniti, D., Ferreira Lopes, C. E., Catelan, M., Minniti, J. H., Nikzat, F., & Zoccali, M. 2019, A&A, 625, A151
Bujarrabal, V. 1994, A&A, 285, 953
Cernicharo, J., Kahane, C., Guelin, M., & Hein, H. 1987, A&A, 181, L9
Churchwell, E., et al. 2009, PASP, 121, 213
Deguchi, S., et al. 2004, PASJ, 56, 261
Deguchi, S., Fujii, T., Izumiura, H., Kameya, O., Nakada, Y., & Nakashima, J. 2000a, ApJS, 130, 351
Deguchi, S., Fujii, T., Izumiura, H., Kameya, O., Nakada, Y., Nakashima, J., Ootsubo, T., & Ukita, N. 2000b, ApJS, 128, 571
Egan, M. P., et al. 2003, VizieR Online Data Catalog, V/114
Engels, D., & Bunzel, F. 2015, A&A, 582, A68
Epchtein, N., et al. 1994, Ap&SS, 217, 3
Fujii, T., Deguchi, S., Ita, Y., Izumiura, H., Kameya, O., Miyazaki, A., & Nakada, Y. 2006, PASJ, 58, 529
Glass, I. S., Matsumoto, S., Carter, B. S., & Sekiguchi, K. 2001, MNRAS, 321, 77

Glass, I. S., Whitelock, P. A., Catchpole, R. M., & Feast, M. W. 1995, MNRAS, 273, 383
Gutermuth, R. A., & Heyer, M. 2015, AJ, 149, 64
Habing, H. J. 1996, A&A Rev., 7, 97
Haikala, L. K., Nyman, L. A., & Forsstroem, V. 1994, A&AS, 103, 107
Herwig, F. 2005, ARA&A, 43, 435
Imai, H., et al. 2002, PASJ, 54, L19
Izumiura, H., Deguchi, S., & Fujii, T. 1998, ApJ, 494, L89
Khouri, T., Velilla-Prieto, L., De Beck, E., Vlemmings, W. H. T., Olofsson, H., Lankhaar, B., Black, J. H., & Baudry, A. 2019, A&A, 623, L1
Lane, A. P. 1982, PhD thesis, Massachusetts University
Lewis, B. M. 1989, ApJ, 338, 234
Li, J., An, T., Shen, Z.-Q., & Miyazaki, A. 2010, ApJ, 720, L56
Lindqvist, M., Habing, H. J., & Winnberg, A. 1992, A&A, 259, 118
Lindqvist, M., Ukita, N., Winnberg, A., & Johansson, L. E. B. 1991, A&A, 250, 431
Lucas, P. W., et al. 2008, MNRAS, 391, 136
Lumsden, S. L., Hoare, M. G., Oudmaijer, R. D., & Richards, D. 2002, MNRAS, 336, 621
Matsunaga, N., Kawadu, T., Nishiyama, S., Nagayama, T., Hatano, H., Tamura, M., Glass, I. S., & Nagata, T. 2009, MNRAS, 399, 1709
Messineo, M. 2004, PhD thesis, Leiden University
Messineo, M., Habing, H. J., Menten, K. M., Omont, A., & Sjouwerman, L. O. 2004, A&A, 418, 103
Messineo, M., Habing, H. J., Menten, K. M., Omont, A., Sjouwerman, L. O., & Bertoldi, F. 2005, A&A, 435, 575
Messineo, M., Habing, H. J., Sjouwerman, L. O., Omont, A., & Menten, K. M. 2002, A&A, 393, 115
Messineo, M., Habing, H. J., Sjouwerman, L. O., Omont, A., & Menten, K. M. 2018, A&A, 619, A35
Nyman, L.-A., Hall, P. J., & Le Bertre, T. 1993, A&A, 280, 551
Nyman, L.-A., Johansson, L. E. B., & Booth, R. S. 1986, A&A, 160, 352
Omont, A., et al. 2003, A&A, 403, 975
Ortiz, R., et al. 2002, A&A, 388, 279
Price, S. D., Egan, M. P., Carey, S. J., Mizuno, D. R., & Kuchar, T. A. 2001, AJ, 121, 2819
Qiao, H.-H., et al. 2018, ApJS, 239, 15
Samus', N. N., Kazarovets, E. V., Durlevich, O. V., Kireeva, N. N., & Pastukhova, E. N. 2017, Astron. Rep., 61, 80
Schuller, F., et al. 2003, A&A, 403, 955
Sevenster, M. N. 2002, AJ, 123, 2772
Sevenster, M. N., Chapman, J. M., Habing, H. J., Killeen, N. E. B., & Lindqvist, M. 1997, A&AS, 122, 79
Sevenster, M. N., van Langevelde, H. J., Moody, R. A., Chapman, J. M., Habing, H. J., & Killeen, N. E. B. 2001, A&A, 366, 481
Shiki, S., & Deguchi, S. 1997, ApJ, 478, 206
Sjouwerman, L. O., Capen, S. M., & Claussen, M. J. 2009, ApJ, 705, 1554
Sjouwerman, L. O., Lindqvist, M., van Langevelde, H. J., & Diamond, P. J. 2002, A&A, 391, 967
Sjouwerman, L. O., van Langevelde, H. J., Winnberg, A., & Habing, H. J. 1998, A&AS, 128, 35
Skrutskie, M. F., et al. 2006, AJ, 131, 1163
Sloan, G. C., Kraemer, K. E., Price, S. D., & Shipman, R. F. 2003, ApJS, 147, 379
Stroh, M. C., Pihlström, Y. M., Sjouwerman, L. O., Claussen, M. J., Morris, M. R., & Rich, M. R. 2018, ApJ, 862, 153
Stroh, M. C., Pihlström, Y. M., Sjouwerman, L. O., Lewis, M. O., Claussen, M. J., Morris, M. R., & Rich, R. M. 2019, ApJS, 244, 25
Urago, R., Omodaka, T., Nagayama, T., Watabe, Y., Miyanosita, R., Matsunaga, N., & Burns, R. A. 2020, ApJ, 891, 50
van der Veen, W. E. C. J., & Habing, H. J. 1988, A&A, 194, 125
Vanhollebeke, E., Blommaert, J. A. D. L., Schultheis, M., Aringer, B., & Lançon, A. 2006, A&A, 455, 645
Vassiliadis, E., & Wood, P. R. 1993, ApJ, 413, 641
Wood, P. R., Habing, H. J., & McGregor, P. J. 1998, A&A, 336, 925
Wright, E. L., et al. 2010, AJ, 140, 1868
Yamamoto, S., Saito, S., Kawaguchi, K., Chikada, Y., Suzuki, H., Kaifu, N., Ishikawa, S.-I., & Ohishi, M. 1990, ApJ, 361, 318